Theor Chem Account (2008) 121:33–41
DOI 10.1007/s00214-008-0443-6

REGULAR ARTICLE

# Theoretical study of the reaction of ethynyl radical with acetonitrile

**Jing-Yu Sun · Yi-Zhen Tang · Hao Sun · Xiu-Juan Jia · Xiu-Mei Pan · Ya-Ru Pan · Rong-Shun Wang**

Received: 8 December 2007 / Accepted: 24 March 2008 / Published online: 17 April 2008


**Abstract** A detailed computational study has been performed on the mechanism and kinetics of the $C_2H$ + $CH_3CN$ reaction. The geometries were optimized at the BHandHLYP/6–311$G(d, p)$ level. The single-point energies were calculated using the BMC-CCSD, MC-QCISD and QCISD(T)/6–311+G($2df$, $2pd$) methods. Five mechanisms were investigated, namely, direct hydrogen abstraction, C-addition/elimination, N-addition/elimination, $C_2H$–to–CN substitution and H-migration. The kinetics of the title reaction were studied using TST and multichannel RRKM methodologies over a wide range of temperatures (150–3,000 K) and pressures ($10^{-4}$–$10^4$ torr). The total rate constants show positive temperature dependence and pressure independence. At lower temperatures, the C-addition step is the most feasible channel to produce $CH_3$ and HCCCN. At higher temperatures, the direct hydrogen abstraction path is the dominant channel leading to $C_2H_2$ and $CH_2CN$. The calculated overall rate constants are in good agreement with the experimental data.

**Keywords** $CH_3CN \cdot C_2H \cdot$ Mechanism · Rate constants

## 1 Introduction

The ethynyl radical ($C_2H$) is known to play an important role in combustion chemistry [1,2]. It has also been detected in interstellar space [3–6] and planetary atmosphere [7,8]. Its low temperature reactivity and kinetics (such as in Titan's atmosphere) have motivated recent studies [9–12]. Acetonitrile, $CH_3CN$, is an important intermediate in combustion processes and a trace gas in the atmosphere [13]. It has also been identified as a component of Titan's atmosphere [14–16]. The reactions of $CH_3CN$ with F, Cl, O($^3$P), OH and H have been well investigated experimentally and theoretically [17–21]. However, the reaction of $CH_3CN$ with $C_2H$, an important reaction in Titan's atmosphere, has rarely been studied. Examination of the literature reveals only two earlier studies of this reaction. In 1997, Hoobler and leone [22] measured the rate coefficients of the $C_2H + CH_3CN \rightarrow$ products and rate constants were (1.0–2.1) $\times 10^{-12}$ cm$^3$ molecule$^{-1}$ s$^{-1}$ over the temperature range of 262–360 K. Nizamov and Leone also measured the rate constants for the title reaction, which were fit to an Arrhenius expression, $k = (1.8 \pm 0.35) \times 10^{-11} \exp(-766 \pm 38/T)$. The rate constant was $(1.35 \pm 0.3) \times 10^{-12}$ cm$^3$ molecule$^{-1}$ s$^{-1}$ at 296 ± 2 K [23]. The following thermodynamic possible channels were proposed via both direct hydrogen abstraction and addition/elimination mechanisms:

$$C_2H + CH_3CN \rightarrow C_2H_2 + CH_2CN \quad \Delta H_r = -180 \text{ kJ/mol}$$
$$C_2H + CH_3CN \rightarrow HCCCN + CH_3 \quad \Delta H_r = -150 \text{ kJ/mol}$$

The motivation of the current study is to characterize the $C_2H$ + $CH_3CN$ reaction on a sound theoretical basis. We carried out detailed ab initio calculations to expatiate the mechanisms for the title reaction as well as the rate constants over a wide range of temperatures (150–3,000 K) and pressures ($10^{-4}$–$10^4$ torr) using the TST and multichannel RRKM theories.

Science Foundation for Young Teachers of Northeast Normal University.

J.-Y. Sun · Y.-Z. Tang · H. Sun · X.-J. Jia · X.-M. Pan · Y.-R. Pan · R.-S. Wang (✉)
Faculty of Chemistry, Institute of Functional Material Chemistry, Northeast Normal University, Renmin Road 5268, Changchun, Jilin 130024, People's Republic of China
e-mail: wangrs@nenu.edu.cn

## 2 Computational methods

All electronic structure calculations were performed using the GAUSSIAN 98 program [24]. For the present open-shell doublet system, the UMP2 method reveals that the wavefunctions are severely contaminated because the expectation values of $S^2$ after annihilation are always around 0.9. It implies that UMP2 calculations could not be reliable. Previous studies showed that the density functional theory (DFT) is capable of annihilating spin contamination effectively [25, 26]. Thus, the geometries of all reactants (R), products (P), intermediates (IM), and transition states (TS) were optimized using the BHandHLYP [27,28] method with the 6–311 $G(d, p)$ basis set. It is encouraging that the expectation values of $S^2$ range from 0.80 to 0.75 before annihilation. After annihilation the values of $S^2$ are always 0.75 (the exact value for a pure doublet is 0.75). Thus, the spin contamination is not severe. Harmonic vibrational frequencies, moments of inertia and zero-point energies (ZPE) were calculated at the same level of theory. The intrinsic reaction coordinate (IRC) calculations at the BHandHLYP/6–311 $G(d, p)$ level have been done to verify the transition states connecting to the desired reactants and products. The geometries optimized at the BHandHLYP/6–311$G(d, p)$ level were used to perform single-point energy calculations for all species using the BMC–CCSD method [29]. In this work, we have also carried out the calculations using MC–QCISD [30] and QCISD(T)/6–311+$G(2df, 2pd)$ (single-point) levels in order to test the accuracy of BMC–CCSD energies. Our calculations indicated that the barriers of the main reaction channels were in good agreement with one another.

The multichannel RRKM calculations were carried out the total and individual rate constants for the important product channels.

## 3 Results and discussion

### 3.1 Reaction mechanism

The BHandHLYP/6–311$G(d, p)$ optimized geometries of reactants, products, intermediates and transition states along with the available experimental values are depicted in Fig. 1, From Fig. 1, we can see that the largest deviations of bond length and angle between theoretical geometrical parameters and experimental values are 0.01 Å and 0.3°, respectively, and the agreements are satisfactory. The schematic potential energy profiles of the title reaction are plotted in Figs. 2 and 3. Table 1 summarizes the ZPE corrections and electronic energies calculated using the BHandHLYP/6–311$G(d, p)$, BMC–CCSD, MC–QCISD and QCISD(T)/6–311+$G(2df, 2pd)$ methods. The moments of inertia and harmonic vibrational frequencies of the key species are listed in Table 2.

For the $C_2H + CH_3CN$ reaction, five mechanisms were studied: direct hydrogen abstraction, C-addition/elimination, N-addition/elimination, $C_2H$–to–CN substitution and H-migration. The detailed reaction mechanisms will be discussed below. The energies discussed in the present work are at the BMC–CCSD + ZPE level, unless otherwise stated.

#### *3.1.1 Direct hydrogen abstraction*

The ethynyl radical exhibits a $^2\sum^+$ electronic ground state in which the unpaired electron is mainly located in the $2p\sigma$ orbital of the terminal carbon atom. The terminal carbon atom can abstract one of hydrogen atoms of the methyl group of the $CH_3CN$ molecule, forming P1 ($C_2H_2 + CH_2CN$) via TS1. The energy of P1 is 35.33 kcal/mol lower than the reactants. In TS1, the forming C–H bond is 1.682 Å, which is 0.626 Å longer than the equilibrium distance of the C–H bond in $C_2H_2$, while the breaking C–H bond is elongated by 0.050 Å. The reacting C–H–C structure is nearly collinear with an angle of 174°. In view of these structural characteristics, TS1 is more reactant-like, which implies that this channel undergoes an early barrier. The relative energy of TS1 is 0.67 kcal/mol.

#### *3.1.2 C-addition/elimination*

The terminal carbon atom in $C_2H$ can add to the C atom of the CN group in $CH_3CN$ via TS2 with the formation of IM1. The forming C–C bond in TS2 is 2.292 Å, which is 0.855 Å longer than that in the IM1. Evidently, TS2 is more reactant-like and an early barrier, in accordance with the reaction exothermicity of 43.14 kcal/mol. Compared with the geometrical parameters of $CH_3CN$, the C–N bond in IM1 turns out to be of double-bond character which is 1.249 Å. The C–C bond is also slightly stretched. The barrier height of TS2 is 0.18 kcal/mol, which is 0.49 kcal/mol lower than the entrance barrier of the direct hydrogen abstraction path. With the internal energy of 43.14 kcal/mol, IM1 dissociates into P2 ($CH_3 + HCCCN$) via TS3. The breaking C–C bond in TS3 is stretched by 0.680 Å compared with that in the IM1. Meanwhile, the C–N bond is shortened, tending to form HCCCN. This bond cleavage path is endothermic by 15.03 kcal/mol despite the overall exothermicity of 28.12 kcal/mol. The calculated barrier height is 24.91 kcal/mol with respect to IM1. This mechanism will compete with direct hydrogen abstraction effectively because of similar and lower entrance barrier.

#### *3.1.3 N-addition/elimination*

The terminal carbon atom in $C_2H$ radical can also add to the nitrogen side of acetonitrile forming the adduct IM2 via

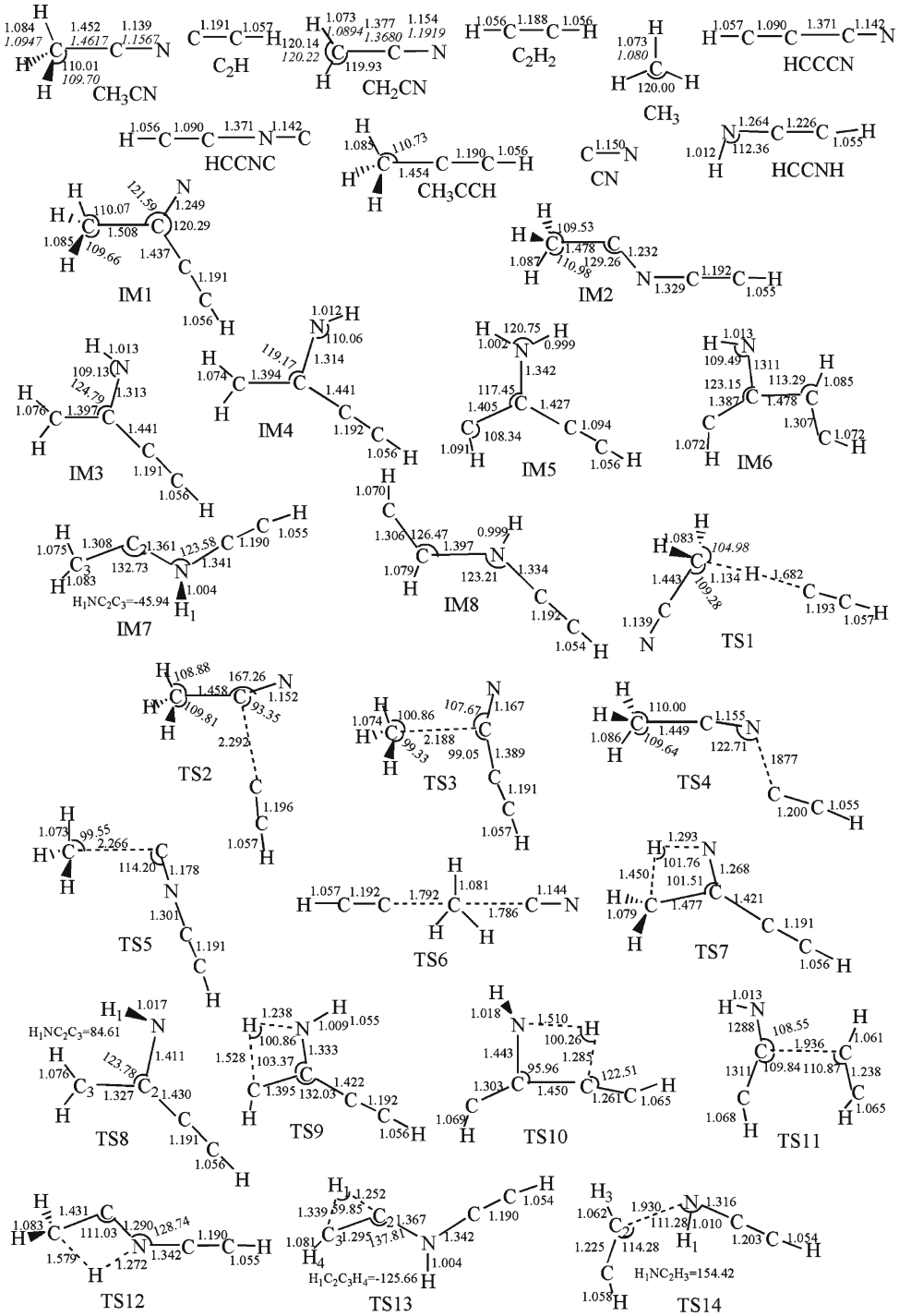


**Fig. 1** Optimized geometries for reactants, products, intermediates and transition states for the $C_2H + CH_3CN$ reaction at the BHandHLYP/6-311$G(d, p)$ level. The values in *italics* correspond to the experimental data [37–39] (bond lengths are given in angstroms and angles in degrees)

TS4. The forming N–C bond in TS4 is 1.877 Å, which is 0.645 Å longer than that in the IM2. The barrier height is 0.65 kcal/mol, similar to the entrance barrier of the direct hydrogen abstraction path and 0.47 kcal/mol higher than of C-addition step. The energy of IM2 is 29.32 kcal/mol lower than reactants, however, 13.82 kcal/mol higher than that of IM1. IM2 can further decompose to form P3 ($CH_3$+HCCNC) via TS5. This is a C–C bond scission process in which the breaking C–C bond is elongated by up to 0.788 Å. The barrier height is 33.45 kcal/mol with respect to IM2. This bond cleavage path is endothermic by 28.20 kcal/mol. Compared with C-addition/elimination, IM2 and P3 are less stable than IM1 and P2. Moreover, the barrier height of TS4 is higher than of TS3. Therefore, the C-addition/elimination mechanism occurs more preferentially than N-addition/elimination mechanism.

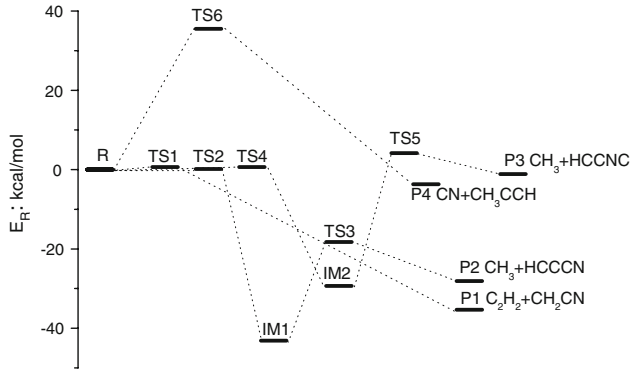


**Fig. 2** The potential energy surface for direct hydrogen abstraction, C-addition/elimination, N-addition/elimination and $C_2H$-to-CN substitution mechanisms at the BMC–CCSD//BHandHLYP/6-311$G(d, p)$ level

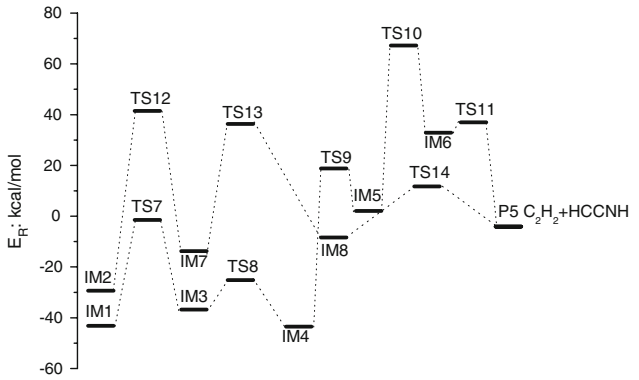


**Fig. 3** The potential energy surface for H-migration mechanism at the level of BMC-CCSD//BHandHLYP/6-311$G(d, p)$

### *3.1.4 $C_2H$-to-CN substitution*

The terminal C atom in $C_2H$ radical attacks to the methyl carbon of $CH_3CN$, kicking off the CN group and forming the $CH_3C_2H$. The transition state for this substitution reaction is TS6 as described in Fig. 1. The forming and breaking C–C bond have the nearly same distance, 1.792 and 1.786 Å, respectively. The barrier height of TS6 is rather high, 35.48 kcal/mol. Moreover, the formation process of P4 (CN + $CH_3CCH$) is faintly exothermic by only 3.68 kcal/mol. Due to the high barrier height, it is anticipated that this elementary substitution channel should play a subordinate role for the title reaction compared with the former three mechanisms.

### *3.1.5 H-migration*

Two possible hydrogen migration pathways were found from IM1 or IM2. The first one is starting from IM1. This hydrogen migration pathway is as follows:

$$\text{IM1} \rightarrow \text{TS7} \rightarrow \text{IM3} \rightarrow \text{TS8} \rightarrow \text{IM4} \rightarrow \text{TS9} \rightarrow \text{IM5} \rightarrow \text{TS10} \rightarrow \text{IM6} \rightarrow \text{TS11} \rightarrow \text{P5}(C_2H_2 + \text{HCCNH})$$

Hydrogen atom of the methyl group is shifted to the N atom, forming planar structural IM3 via a four-center structural TS7. The breaking C–H and forming H–N bond are 1.450 and 1.293 Å. The NCC bond angle in TS7 decreases by up to 20.08° with respect to the IM1. The corresponding barrier height is 41.63 kcal/mol. IM3 can transform to its isomer IM4 via TS8. Thermodynamically, IM4 is about 6.66 kcal/mol more stable than IM3. However, this isomerization is rather difficult to occur because a high barrier (TS8) of 11.66 kcal/mol has to be surmounted. Subsequently, the hydrogen atom of methylene group in IM4 is shifted to the N atom once again leading to IM5 via TS9. The barrier height of TS9 is 62.26 kcal/mol. The breaking C–H and forming H–N bonds are 1.528 and 1.238 Å, respectively. Then the hydrogen atom of the $NH_2$ group in IM5 shifts onto C atom via a four-center transition state TS10, forming IM6. The breaking H–N and forming C–H bonds are 1.510 and 1.285 Å, respectively. The energy barrier is as high as 65.20 kcal/mol. Subsequently, the C–C bond in IM6 will rupture to produce P5 ($C_2H_2$ + HCCNH) via TS11 with the barrier height of 4.04 kcal/mol. The breaking C–C bond is stretched to 1.936 Å. For this channel, the barrier heights of TS9 and TS10 are comparatively higher, 62.26 and 65.20 kcal/mol, and IM5 and IM6 lie well above the reactants. Thus, this path is less competitive.

The second reaction starts from IM2. This reaction is 1,3-H shift from C atom of methyl group to the N atom, leading to IM7 via TS12. The breaking H–C and forming N-H bond are 1.579 and 1.272 Å, respectively. The barrier height is exceedingly high, 70.77 kcal/mol. Subsequently, the hydrogen of methylene group in IM7 is shifted to the neighbor C atom leading to IM8 via a three-center transition state TS13. The breaking and forming H–C bond are 1.339 and 1.252 Å, respectively. The barrier height of TS13 is 50.09 kcal/mol. Subsequently, the N–C bond in IM8 breaking occurs, as indicated by the elongated distance of 1.930 Å, leading to P5 ($C_2H_2$+HCCNH) via TS14 with the barrier height of 20.11 kcal/mol. All barriers for this pathway are greatly higher than the reactants. Thus, this channel is not important to the overall reaction rate.

## 3.2 Rate constants

For the rate constant calculations, we choose three important reaction channels: direct hydrogen abstraction, C-addition/elimination and N-addition/elimination. The following

**Table 1** Relative Energies and ZPE Correction (in kcal/mol) for various species through the $C_2H + CH_3CN$ reaction together with the experimental values

| Species | ZPE | $E_R$(BHandHLYP)[a] | $E_R$(BMC-CCSD)[b] | $E_R$(MC-QCISD)[c] | $E_R$(QCISD(T))[d] | Expt[e] |
|---|---|---|---|---|---|---|
| $CH_3CN + C_2H$(R) | 39.33 | 0.00 | 0.00 | 0.00 | 0.00 | – |
| IM1 | 42.22 | −49.53 | −43.14 | −43.92 | −44.19 | – |
| IM2 | 41.88 | −34.87 | −29.32 | −31.02 | −29.81 | – |
| IM3 | 41.83 | −47.02 | −36.81 | −42.86 | – | – |
| IM4 | 41.99 | −49.00 | −43.47 | −44.54 | – | – |
| IM5 | 43.68 | −2.29 | 2.03 | −0.75 | – | – |
| IM6 | 39.93 | 17.78 | 32.92 | 32.84 | – | – |
| IM7 | 41.80 | −18.65 | −13.76 | −15.33 | – | – |
| IM8 | 41.54 | −14.13 | −8.41 | −10.14 | – | – |
| TS1 | 38.18 | 1.14 | 0.67 | 1.49 | 1.05 | – |
| TS2 | 39.82 | 1.03 | 0.18 | 1.05 | 0.57 | – |
| TS3 | 38.89 | −19.44 | −18.23 | −16.60 | −18.26 | – |
| TS4 | 39.62 | 2.45 | 0.65 | 2.13 | 2.50 | – |
| TS5 | 38.25 | −2.58 | 4.13 | 2.38 | 1.90 | – |
| TS6 | 38.95 | 42.31 | 35.48 | 36.87 | – | – |
| TS7 | 38.73 | −0.56 | −1.51 | −1.23 | – | – |
| TS8 | 41.17 | −32.39 | −25.15 | −28.59 | – | – |
| TS9 | 38.28 | 16.32 | 18.79 | 16.04 | – | – |
| TS10 | 36.02 | 62.33 | 67.23 | 71.71 | – | – |
| TS11 | 37.38 | 32.20 | 36.96 | 40.90 | – | – |
| TS12 | 37.32 | 40.24 | 41.45 | 39.56 | – | – |
| TS13 | 37.98 | 33.19 | 36.33 | 33.28 | – | – |
| TS14 | 38.75 | 11.28 | 11.70 | 12.45 | – | – |
| P1($C_2H_2 + CH_2CN$) | 37.71 | −41.02 (−40.97) | −35.33 (−35.28) | −38.09 (−39.67) | −37.15 (−37.10) | −43.02 |
| P2 ($CH_3$ + HCCCN) | 36.92 | −32.83 (−32.36) | −28.12 (−27.65) | −31.03 (−32.97) | −30.75 (−30.28) | −35.85 |
| P3 ($CH_3$ + HCCNC) | 36.44 | −8.83 | −1.12 | −4.45 | −4.28 | – |
| P4 (CN + $CH_3CCH$) | 39.36 | 0.89 | −3.68 | −4.30 | – | – |
| P5 ($C_2H_2$ + HCCNH) | 36.89 | −9.08 | −4.08 | −6.78 | – | – |

[a] At the BHandHLYP/6–311G(d, p)+ZPE level
[b] At the BMC-CCSD+ZPE level
[c] At the MC-QCISD+ZPE level
[d] At the QCISD(T)/6–311+G(2df, 2pd)+ZPE level
[e] Experimental enthalpies of formation at 298 K are taken from [22,23]. The values in the *parentheses* are the calculated reaction enthalpies

reaction paths are included in the calculations:

$$\text{Mechanism I}: \quad C_2H + CH_3CN \xrightarrow{TS1} C_2H_2 + CH_2CN\ (P1)$$

$$\text{Mechanism II}: \quad C_2H + CH_3CN \underset{2}{\overset{1(TS2)}{\rightleftharpoons}} \begin{matrix} CH_3C(CCH)N^*(IM1^*) \\ \downarrow \omega \\ CH_3C(CCH)N(IM1) \end{matrix} \xrightarrow{3(TS3)} CH_3 + HCCCN\ (P2)$$

$$\text{Mechanism III}: \quad C_2H + CH_3CN \underset{5}{\overset{4(TS4)}{\rightleftharpoons}} \begin{matrix} CH_3CN(CCH)^*(IM2^*) \\ \downarrow \omega \\ CH_3CN(CCH)(IM2) \end{matrix} \xrightarrow{6(TS5)} CH_3 + HCCNC\ (P3)$$

where " $*$ " represents the vibrational excitation of the intermediates.

Conventional transition state theory (CTST), including the unsymmetrical Eckart tunneling correction [31] is employed to estimate the rate constants for mechanism I. For mechanisms II and III, the multichannel RRKM theory is used [32]. During the rate-constant calculations, single-point energies of all species for three mechanisms are found at the

**Table 2** Moments of inertia ($I_a$, $I_b$, $I_c$, in amu) and harmonic vibrational frequencies (in $cm^{-1}$) of the key species for the important channels through the $C_2H$ with $CH_3CN$ reaction at the BHandHLYP/6-311$G(d, p)$ level

| Species | $I_a$, $I_b$, $I_c$ | Frequencies |
|---|---|---|
| $CH_3CN$ | 11.2, 192.5, 192.5 | 408 (362)[a], 960 (920), 1104 (1041), 1466 (1381), 1528 (1448), 2489 (2266), 3139 (2954), 3216 (3009) |
| $C_2H$ | 0.0, 39.8, 39.8 | 614, 618, 2164, 3549 |
| $CH_2CN$ | 6.2, 173, 179 | 409 (367), 459 (437), 682 (680), 1073 (1041), 1079 (1124), 1494, 2209 (2156), 3252, 3364 (3301) |
| $C_2H_2$ | 0.0, 49.8, 49.8 | 726, 817, 2147, 3504, 3613 |
| $CH_3$ | 6.2, 6.2, 12.4 | 497 (606), 1452 (1402), 3189 (3004), 3373 (3171) |
| HCCCN | 0.0, 389.2, 389.2 | 253, 585, 776, 925, 2272, 2508, 3558 |
| HCCNC | 0.0, 357.1, 357.1 | 236, 510, 734, 996, 2216, 2414, 3569 |
| IM1 | 165.6, 438.7, 593.2 | 173, 188, 273, 406, 574, 592, 756, 760, 787, 1051, 1080, 1208, 1446, 1525,1528, 1768, 2300, 3128, 3198, 3228, 3561 |
| IM2 | 24.3, 761.8, 775.1 | 138, 152, 165, 430, 511, 566, 662, 731, 876,1047, 1129, 1138, 1438, 1510, 1516,1912, 2313, 3106, 3188, 3190, 3575 |
| TS1 | 112.9, 1084.5,1185.9 | 242i[b], 44, 63, 107, 251, 409, 420, 669, 671, 972, 1078, 1096, 1372,1417, 1496, 2007, 2197, 2477, 3174, 3238, 3547 |
| TS2 | 194.9, 563.6, 747.4 | 321i, 58, 70, 137, 219, 318, 412, 687, 693, 937, 1082, 1111, 1462, 1519, 1524,2134, 2340, 3144, 3226, 3232, 3548 |
| TS3 | 228.2, 449.9, 666.0 | 592i, 85, 160, 257, 307, 475, 505, 602, 626, 739, 774, 889, 979, 1462, 1474, 2111,2338, 3172, 3336, 3349, 3560 |
| TS4 | 65.3, 833.5, 887.6 | 387i, 45, 67, 70, 215, 422, 424, 693, 719, 937, 1080, 1104, 1459, 1517, 1519,2095, 2262, 3123, 3197, 3216, 3549 |
| TS5 | 98.2, 777.8, 863.8 | 352i, 26, 75, 240, 270, 479, 480, 520, 522, 687, 733, 841, 1004, 1460, 1470, 2139, 2362, 3178, 3343, 3359, 3571 |

[a] The experimental vibrational frequencies are listed by *Italics* in brackets [40–42]
[b] i represents imaginary frequency

BMC–CCSD level. It is in view of two aspects in the accuracy of the calculations at the BMC-CCSD level: (i) The mean unsigned error for barrier height is only 0.71 kcal/mol [29]; and (ii) The rate constant is determined mainly by the barrier height, and the calculated entrance barrier of 0.18 kcal/mol (C-addition/elimination mechanism) is in good agreement with experimental value of 0.29 kcal/mol [23]. Therefore, the calculations of BMC–CCSD are the most appropriate to the title reaction. Steady-state assumption for excited intermediates leads to the following expressions for the second-order rate coefficients of mechanism Π as an example:

$$k_{P2}(E) = \frac{\alpha}{h}\frac{Q_t^{\neq}Q_r^{\neq}}{Q_{C_2H}Q_{CH_3CN}}\mathrm{e}^{-Ea/(RT)} \times \int_0^{\infty}\frac{k_3 N_2(E^{\neq})}{k_2+k_3+\omega}\mathrm{e}^{-E^{\neq}/RT}\mathrm{d}E^{\neq}$$

$$k_{\mathrm{IM1}}(E) = \frac{\alpha}{h}\frac{Q_t^{\neq}Q_r^{\neq}}{Q_{C_2H}Q_{CH_3CN}}\mathrm{e}^{-Ea/(RT)} \times \int_0^{\infty}\frac{\omega N_2(E^{\neq})}{k_2+k_3+\omega}\mathrm{e}^{-E^{\neq}/RT}\mathrm{d}E^{\neq}$$

$$k_{II}(E) = \frac{\alpha}{h}\frac{Q_t^{\neq}Q_r^{\neq}}{Q_{C_2H}Q_{CH_3CN}}\mathrm{e}^{-Ea/(RT)} \times \int_0^{\infty}\frac{(k_3+\omega)N_2(E^{\neq})}{k_2+k_3+\omega}\mathrm{e}^{-E^{\neq}/RT}\mathrm{d}E^{\neq}$$

where $\alpha(\alpha = 2)$ is the statistical factor (degeneracy) for the reaction step 1; $E_a$ is the energy barrier of TS2 for the reaction step 1; $Q_{C_2H}$ and $Q_{CH_3CN}$ are the total partition function of $C_2H$ and $CH_3CN$, respectively; $Q_t^{\neq}$ and $Q_r^{\neq}$ are the translational and rotational partition functions of the transition state TS2 for the association; $N_2(E^{\neq})$ is the number of state for the association transition state (TS2) with excess energy $E^{\neq}$ above the association barrier.

The microcannonical rate constant is calculated using RRKM theory as follows:

$$k_i(E) = \alpha_i\kappa\sqrt{I_i^{\neq}/I_j^{\mathrm{IM}}}\frac{N_i(E-E_i^{\neq})}{h\rho_j(E)}, \quad i = 1, 2; \quad j = 1$$

where $k_i(E)$ is the energy-specific rate constant for the $i$th channel; $\alpha_i$ is the statistical factor for reaction path degeneracy; $\kappa$ is the tunneling factor; $I_i^{\neq}$, $I_j^{\mathrm{IM}}$ is the moments of

inertia ($I_a I_b I_c$) of the transition state $i$ and the intermediate $j$; $h$ is Planck's constant; $\rho_j(E)$ is the density of states at energy $E$ of the intermediate $j$; $N_i(E - E_i^{\neq})$ is the number of states at the energy above the barrier height for transition state $i$; The density of states and the number of states are calculated using the extended Beyer–Swinehart algorithm [33,34]. The collision deactivation rate is $\omega = \beta_c Z_{LJ}[\mathrm{M}]$, where $\beta_c$ is the collision efficiency calculated using Troe's weak collision approximation with the energy transfer parameter $-\langle\Delta E\rangle$. The temperature-dependent energy-transfer parameter $-\langle\Delta E\rangle$ is estimated by Lim and Gilbert's biased random walk (BRW) model ($T$ = 200–1,000 K) [35]: $-\langle\Delta E\rangle/\ \mathrm{cm}^{-1} = 0.52T + 6$ for nitrogen. In consideration of the experimental rate constants measured at different pressures, it is found that the values around 160 $\mathrm{cm}^{-1}$ for $-\langle\Delta E\rangle$ should be reasonable to calculate the rate constants. It is worth noting that the overall rate constant is not sensitive to the $-\langle\Delta E\rangle$ parameter. $Z_{LJ}$ is the Lennard–Jones collision frequence. The collision efficiency is estimated using the Lennard–Jones potential ($V(r) = 4\varepsilon[(\sigma/r)^{12} - (\sigma/r)^6]$) by fitting the interaction energies calculated at the BHandHLYP/6–311$G(d, p)$ level for IM1...$N_2$ and IM2...$N_2$. It is estimated that ($\varepsilon$ = 70.24 K, $\sigma$ = 3.41 Å) for IM1...$N_2$ and ($\varepsilon$ = 22.81 K, $\sigma$ = 3.96 Å) for IM2...$N_2$, and [M] is the concentration of the bath gas M ($N_2$). The weak collision approximation is used for each intermediate.

The rate constants for the direct hydrogen abstraction can be readily obtained using the conventional transition-state theory [36]:

$$k_{\mathrm{abs}}(T) = \kappa_1 \frac{k_B T}{h} \frac{Q_{TS1}^{\neq}}{Q_{C_2H} Q_{CH_3CN}} \mathrm{e}^{-E_1/(RT)}$$

where $\kappa_1$ is the tunneling factor, $k_B$ and $h$ are Boltzmann and Planck constants, respectively. $Q_{TS1}^{\neq}$, $Q_{C_2H}$, and $Q_{CH_3CN}$ are the TS1, $C_2H$ and $CH_3CN$ partition functions. $E_1$ is the energy barrier of TS1.

The calculated rate constants for the formation channels of P1, P2, P3, IM1 and IM2 are denoted as $k_{P1}, k_{P2}$, $k_{P3}$, $k_{IM1}$ and $k_{IM2}$, respectively. The total second-order rate constant for the $C_2H + CH_3CN$ reaction is noted as $k$, $k = k_{P1} + k_{P2} + k_{P3} + k_{IM1} + k_{IM2}$. The branching ratios are $k_{P1}/k$, $k_{P2}/k$, $k_{P3}/k$, $k_{IM1}/k$ and $k_{IM2}$/k, respectively.

### 3.2.1 Temperature dependence

Figure 4 shows the total and individual rate constants over the temperature range of 150–3,000 K and at a pressure of 1 torr in order to compare with the previous experimental results. As seen in Fig. 4, the total rate constants of the title reaction show strong positive temperature dependence. The predicted total rate constants are in good agreement with the available experimental data. For example, at 296 K, the calculated total rate constant is $1.74 \times 10^{-12}$ $\mathrm{cm}^3$ $\mathrm{molecule}^{-1}$ $\mathrm{s}^{-1}$, which is in excellent agreement with the experimental value of $1.35 \times 10^{-12}$ $\mathrm{cm}^3$ $\mathrm{molecule}^{-1}$ $\mathrm{s}^{-1}$[23]. At lower temperatures, 150–360 K, $k_{P2}$ is much higher than $k_{P1}, k_{P3}, k_{IM1}$ and $k_{IM2}$. The product P2 ($CH_3$ + HCCCN) is more important than the stabilized IM1 in kinetic studies. This result is not hard to understand, which is in view of the energies of TS2, IM1, TS3 and P2. The energies of IM1, TS3 and P2 lie well below the reactants and IM1 has enough energy to climb a barrier of 24.91 kcal/mol. Thus, IM1 can dissociate to form P2 through molecule collision. The branching ratios shown in Fig. 5 show that the $k_{P2}/k$ is approximately from 80 to 50% and the $k_{IM2}/k$ is nearly from 20 to 30% between 150 and 360 K. The $k_{P1}/k$, $k_{IM1}/k$, and $k_{P3}/k$ are much smaller than $k_{P2}/k$. Thus, the title reaction is dominated by mechanism II and the major products are $CH_3$

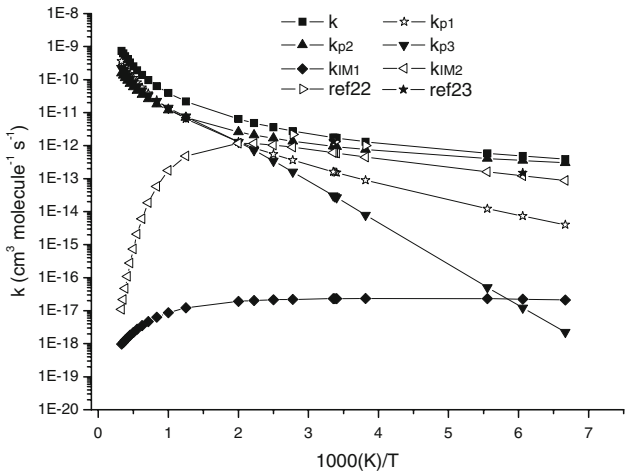


**Fig. 4** The total and individual rate constants along with the experimental values for the $C_2H + CH_3CN$ reaction at the pressure of 1 torr and the temperatures from 150 to 3,000 K

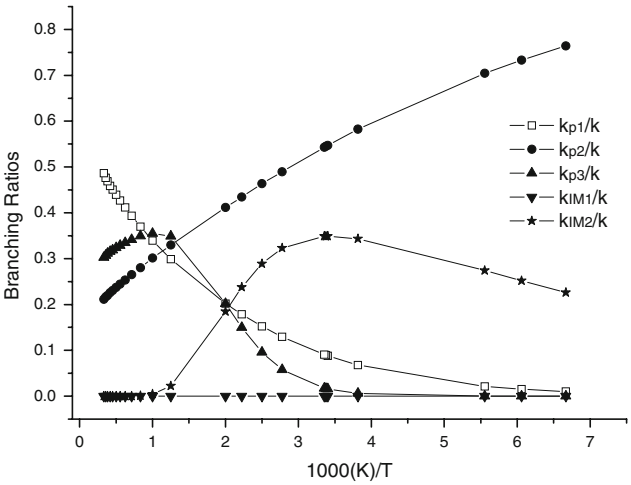


**Fig. 5** The calculated branching ratios of the important channels for the title reaction versus 1,000(K)/T between 150 and 3,000 K at the pressure of 1 torr

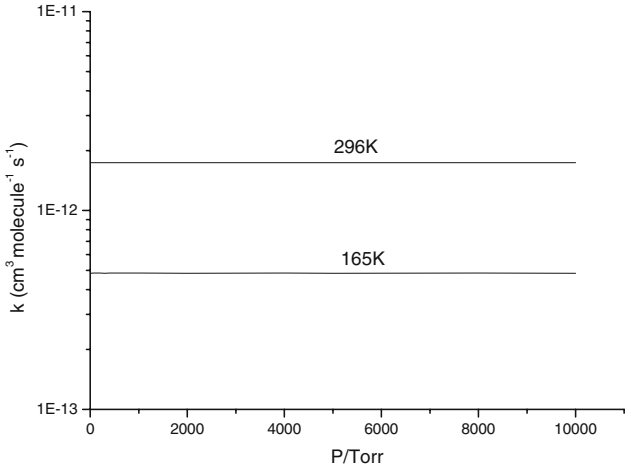


**Fig. 6** Pressure dependence of the overall rate constants for the $C_2H + CH_3CN$ reaction using nitrogen as bath gas at 165 and 296 K with the pressure varying from $10^{-4}$ to $10^4$ torr

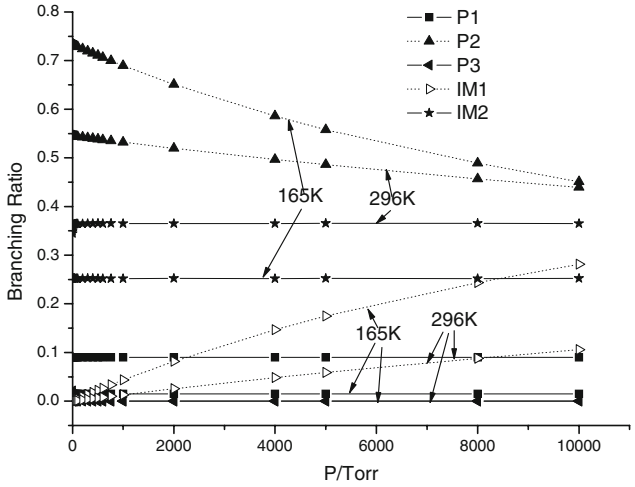


**Fig. 7** Branching ratios of P1, P2, P3, IM1, and IM2 from the $C_2H + CH_3CN$ reaction at 165 and 296 K over the pressure range of $10^{-4}$–$10^4$ torr

and HCCCN at lower temperatures. Moreover, the stabilization of IM2 channel will compete with mechanism II. With the increase in temperature, direct H-abstraction channel will be a strong competitive channel, especially when the temperature is higher than 1,000 K. The branching ratios of $k_{P1}/k$ and $k_{P3}/k$ are approximately 50 and 30% at 3,000 K, respectively. The branching ratios of $k_{P2}/k$, $k_{IM1}/k$, and $k_{IM2}/k$ are smaller than the values of $k_{P1}/k$ and $k_{P3}/k$. Apparently, mechanism I, namely, direct H-abstraction, dominates the overall reaction at the temperatures above 1,000 K. And the product P3 ($CH_3$ + HCCNC) channel will compete with mechanism I. Thus, it can be expected that the major products for the title reaction might be $CH_3$ + HCCCN at lower temperatures (Titan's atmosphere) and $C_2H_2 + CH_2CN$ are the major products at higher temperatures (combustion condition).

### *3.2.2 Pressure dependence*

We have performed a priori calculation for the total rate constants and branching ratios over a wide pressure range of $10^{-4}$–$10^4$ torr at the selected temperatures 165 and 296 K. The results are shown in Figs. 6 and 7, respectively.

From Fig. 6 we can see that the total rate constants show pressure independence. As seen in Fig. 7, the yields of P1, P3 and IM2 are not affected by pressure. The branching ratios of P2 and IM1 vary with pressure. It is worth noting that the yield of P2 decreases as the pressure increases, whereas the yield of IM1 increases as the pressure increases. At 165 K, the yield of P2 is approximately from 75 to 45% between $10^{-4}$ and $10^4$ torr, and the yield of IM1 is from 0.1 to 30%. The calculated results imply that the stabilization of the IM1 adduct becomes important for the title reaction at higher pressures.

## 4 Conclusion

A detailed theoretical study has been carried out on the mechanism and kinetics of the $C_2H + CH_3CN$ reaction at the BMC–CCSD//BHandHLYP/6–311$G(d, p)$ level .The main results can be summarized as follows:

1. The title reaction proceeds via five mechanisms: direct hydrogen abstraction, C-addition/elimination, N-addition/elimination, $C_2H$–to–CN substitution and H-migration mechanisms. The C-addition/elimination, N-addition/elimination and direct hydrogen abstraction channels are important thermodynamically and kinetically. Due to high barriers, the latter two mechanisms play secondary roles for the whole reaction.
2. A trace species in the atmosphere of Titan, HCCCN, would be formed via C-addition/elimination mechanism, which should be helpful for future experimental identification.
3. The rate-constant calculations show that the overall rate constants have a positive temperature dependence and pressure independence. At lower temperatures, the C-addition step is the most favorable and the major products are $CH_3$ and HCCCN. However, at higher temperatures, the direct hydrogen abstraction channel, leading to $C_2H_2 + CH_2CN$ is dominant.

**Acknowledgments** This work is supported by the National Natural Science Foundation of China (No. 20773021) and the Science Foundation for Young Teachers of Northeast Normal University (No. 20070315). The authors are thankful for the reviewer's invaluable comments.

## References


1. Shaub WM, Bauer SH (1978) Combust Flame 32:35
2. Boullart W, Devriendt K, Borms R, Peeters J (1996) J Phys Chem 100:998
3. Tucker KD, Kutner ML, Thaddeus P (1974) Astrophys J 193:L115
4. Jackson WM, Bao YH, Urdahl RS (1991) J Geophys Res 96:17569
5. Hasegawa TI, Kwok S (2001) Astrophys J 562:824
6. Markwick AJ, Hgner M, Millar TJ, Henning T (2001) Astron Astrophys 385:632
7. Strobel DF (1982) Planet Space Sci 30:839
8. Allen M, Yung YL, Gladstone GR (1992) Icarus 100:527
9. Opansky BJ, Leone SR (1996) J Phys Chem 100:4888
10. Hoobler RJ, Opansky BJ, Leone SR (1997) J Phys Chem A 101:1338
11. Stahl F, Schleyer HF, Bettinger RI, Kaiser YT et al (2001) J Chem Phys 114:3476
12. Vakhtin AB, Heard DE, Smith IWM, Leone SR (2001) Chem Phys Lett 21:348
13. Hamm S, Warneck P (1990) J Geophys Res 95:20593
14. Coustenis A (1990) Ann Geophys 8:645
15. Coustenis A, Bezard B, Gautier D, Marten A, Samuelson R (1991) Icarus 89:152
16. Bezard B, Marten A, Paubert G (1993) Bull Am Astron Soc 25:1100
17. Tyndall GS, Orlando JJ, Wallington TJ, Sehested J, Nielsen OJ (1996) J Phys Chem 100:660
18. Budge S, Roscoe JM (1995) Can J Chem 73:666
19. Galano A (2007) J Phys Chem A 111:5086
20. Tyndall GS, Orlando JJ, Wallington TJ, Hurley MD (2001) J Phys Chem A 105:5380
21. Wang BS, Hou H, Gu YS (2001) J Phys Chem A 105:156
22. Hoobler RJ, Leone SR (1997) J Geophys Res [Planets] 102:28717
23. Nizamov B, Leone SR (2004) J Phys Chem A 108:1746
24. Frisch MJ, Trucks GW, Schlegel HB, Scuseria GE, Robb MA, Cheeseman JR, Zakrzewski VG, Montgomery JA, Stratmann RE, Burant JC, Dapprich S, Millam JM, Daniels AD, Kudin KN, Strain MC, Farkas O, Barone V, Cossi M, Cammi R, Mennucci B, Pomelli C, Adamo C, Clifford S, Ochterski J, Petersson GA, Ayala PY, Cui Q, Morokuma K, Malick DK, Rabuck AD, Raghavachari K, Foresman JB, Cioslowski J, Ortiz JV, Stefanov BB, Liu G, Liashenko A, Piskorz P, Komaromi I, Gomperts R, Martin RL, Fox DJ, Keith T, Al-Laham MA, Peng CY, Nanayakkara A, Gonzalez C, Challacombe M, Gill PMW, Johnson BG, Chen W, Wong MW, Andres JL, Head-Gordon M, Replogle ES, Pople JA (1998) Gaussian, Inc., Pittsburgh, PA, Revision A.9
25. Baker J, Scheiner AC, Andzelm JJ (1993) Chem Phys Lett 216:380
26. Baker J, Muir M, Andzelm JJ (1995) J Chem Phys 102:2065
27. Becke AD (1993) J Chem Phys 98:1372
28. Lee C, Yang W, Parr RG (1988) Phys Rev B 37:785
29. Lynch BJ, Zhao Y, Truhlar DG (2005) J Phys Chem A 109:1643
30. Patton LF, Truhlar DG (2000) J Phys Chem A 104:6111
31. Johnston HS, Heicklen J (1962) J Phys Chem 66:532
32. Holbrook KA, Pilling MJ, Robertson SH (1996) Unimolecular reactions. Wiley, Chichester
33. Stein SE, Rabinovitch BS (1973) J Chem Phys 58:2438
34. Astholz DC, Troe J, Wieters W (1979) J Chem Phys 70:5107
35. Lim KF, Gilbert RG (1990) J Chem Phys 92:1819
36. Smith IWM (1980) Kinetics and dynamics of elementary gas reactions. Butterworth, London, p 118
37. Liu YP, Lynch GC, Troung TN, Lu DH, Truhlar DG, Garrett BC (1993) J Am Chem Soc 115:2408
38. Demaison J, Durbrulle A, Boucher D, Burie J, Typke V (1979) J Mol Spectosc 76:1
39. Lide DR (1992) CRC handBook of chemistry and physics, 73rd edn. CRC Press, Boca Raton
40. Holzinger R, Warneke C, Hansel A, Jordan A, Lindinger W (1999) Geophys Res Lett 26:2261
41. Sumiyoshi Y, Tanaka K, Tanaka T (1996) J Chem Phys 104:1839
42. Affefy HY, Liebman JF, Stein SE NIST Chemistry WebBook, NIST Standard Reference Database, http://webbook.nist.gov